ingegneria sismica
International Journal of Earthquake Engineering
Anno XLIII - Num. 2 - 2026

Fatigue life prediction and optimization of wind turbine blade composite under multi-scale finite element simulation

Muhua Niu[1] *and Cheng Chen*[2,*]

[1] School of Intelligent Construction, Wuxi Taihu University, Wuxi, 214000, Jiangsu, China
[2] School of Intelligent Equipment Engineering, Wuxi Taihu University, Wuxi, 214000, Jiangsu, China

SUMMARY: *In this paper, a multi-scale finite element driven framework for fatigue life prediction and parameter optimization of wind turbine blade composites is constructed. For the stress transfer between layers, interface damage evolution and stiffness degradation process, the finite element model is established and the life samples are formed. The dual-branch feature mapping and life prediction module is designed, the parameters, damage variables, strain energy density and load spectrum statistics are uniformly coded, and the adaptive particle search is combined to complete the parameter optimization. Experimental results show that compared with BP regression network, random forest regression and LSTM time series regression model, the absolute percentage error of the test set of the proposed method is 4.87%and the determination coefficient is 0.941. After optimization, the blade mass is reduced by 5.75%, the residual fatigue life is increased by 10.34%, and the constraint satisfaction rate is 96.8%. The results show that the proposed framework can provide computational support for wind turbine blade fatigue assessment and design.*

KEYWORDS: *Multi-scale finite element; Wind turbine blade composite material; Fatigue life prediction; Parameter optimization*

1 Introduction

Wind turbine blade is the core of load bearing and force transmission in wind energy conversion system. The fatigue life, stiffness retention capacity and safety reserve of wind turbine blade in service phase are jointly determined by composite layer structure, local geometric parameters and cyclic load response. As the scale of the blade continues to increase, the empirical analysis at a single scale is difficult to fully characterize the response transfer relationship between the fiber layer, the interface area and the overall structure. The fatigue life calculation based on multi-scale finite element simulation has gradually become an important technical path for blade structure assessment. In this process, the computer modeling method undertakes the tasks of sample generation, feature mapping, life prediction and parameter optimization, which makes the blade fatigue analysis further move from traditional numerical calculation to the technical form of data-driven and intelligent decision-making cooperation. Focusing on wind turbine blade health state recognition, composite material response perception and life estimation, related research has formed a relatively clear algorithm context, and provides a available basis for the establishment of fatigue life prediction and structural optimization methods.

*kercc85@163.com
https://doi.org/10.65102/is2026552
Published: 30 April, 2026

Wang et al. studied the fault detection task of wind turbine blades, and used multi-channel convolutional neural network to process multi-source state signals to realize the automatic identification of abnormal patterns of wind turbine blades [1]. Zhang et al. proposed a leaf defect image recognition method based on attention mechanism, MobileNetv1-YOLOv4 and transfer learning to improve the defect localization effect under complex backgrounds [2]. Xiaoxun et al. studied the wind turbine blade crack detection method based on deep learning, and combined visual feature extraction with the crack recognition model to enhance the surface damage recognition ability [3]. Khazaee et al. studied the blade structural health monitoring method under the condition of tower layout sensing, and used machine learning to complete the operation state analysis of wind turbine blades [4]. Luo et al. proposed a health monitoring method for carbon fiber composite laminated structures of offshore wind turbine blades, and realized the state characterization of composite laminates through double maximum correlation coefficient modeling [5]. Ogaili et al. studied the multi-fault detection method of wind turbine blades based on vibration signals and machine learning, so that multiple types of fault states have a unified identification path [6]. Oliveira-Filho et al. proposed an interpretable supervised variational autoencoder model for early detection and diagnosis of abnormal working conditions of wind turbines, which improved the interpretability of state discrimination [7]. Feng et al. studied the structural health monitoring method of full-size in-service wind turbine blades based on stereo digital image correlation, which expanded the data sources of blade deformation and damage observation [8]. Hang et al. proposed a blade crack monitoring method that integrates classification, detection, segmentation and fault grade assessment, so that the artificial intelligence model can cover the complete process from crack recognition to grade determination [9]. Ye et al. studied the wind turbine blade defect detection method under the framework of semi-supervised deep learning, which maintained good recognition ability under the condition of limited labeled samples [10].

The above studies provide diversified technical support for wind turbine blade state recognition and damage detection, and also show that deep learning, machine learning and visual computing have become an important part of wind turbine blade health assessment. At the same time, the fatigue life prediction and structural parameter optimization still need to integrate the multi-scale finite element calculation results with the intelligent model more closely. The blade composite exhibits the characteristics of parallel evolution of stress transfer between layers, local damage expansion and global stiffness degradation under cyclic loading. It is difficult to directly form a continuous mapping to the life change process by simply relying on external observation signals or single detection results. The information of stress, strain, damage factor, layup parameters and load spectrum generated by finite element simulation is organized into learnable samples, and then the nonlinear mapping relationship between characteristics and life is established through the calculation model, which is helpful to bring structural analysis, fatigue assessment and parameter optimization into a unified calculation framework.

Based on this, this paper focuses on the task of fatigue life prediction and optimization of wind turbine blade composite materials, and constructs a multi-scale finite element driven calculation method. Firstly, the multi-scale fatigue simulation is carried out on the key area of the blade to obtain the life samples and structural response data, and then the life prediction and parameter optimization module under the finite element feature mapping is established to realize the integrated calculation of blade fatigue life estimation and structural parameter optimization. This method is beneficial to enhance the digital expression ability of composite material fatigue analysis, and provide a computable and verifiable technical basis for wind turbine blade structure design. The paper is divided into five parts. The first part is the

introduction, which explains the research background and related progress of fatigue life prediction and optimization of wind turbine blade composite materials. Section II is related work, combing wind turbine blade damage identification, life assessment and intelligent modeling methods. The third part is the fatigue life prediction and optimization method of wind turbine blade composite materials, introducing multi-scale finite element fatigue simulation, life sample construction, and prediction and optimization module design. Section IV shows the experimental results, analyzing the model training, life prediction results and structural parameter optimization performance. Section 5 is the discussion and conclusion, which summarizes the computational performance and application value of the proposed method.

2 Related work

Fatigue life prediction and optimization of wind turbine blade composite materials involve many technologies such as structural mechanics, material damage evolution, numerical simulation and intelligent calculation. As the length of blade, the complexity of load spectrum and the coupling degree of service environment continue to increase, the research path relying only on appearance detection or local signal discrimination is difficult to directly support the integrated calculation of life prediction and parameter optimization. Related research has gradually extended from defect recognition to damage characterization, state estimation, fatigue modeling and intelligent inference, which lays a foundation for the computational framework driven by multi-scale finite element.

Rizk et al. studied the wind turbine blade detection method based on the combination of hyperspectral imaging and 3D convolutional neural network, and realized the fine identification of blade damage area [11]. Davis et al. proposed a blade fault identification and location method based on deep learning, so that cracks, denuding and local anomalies have a unified discriminant path [12]. Yang et al. studied a leaf anomaly detection model combining variational autoencoder and ordinary differential equation, which enhanced the continuous expression ability of the state change process [13]. Sethi et al. proposed a vibration diagnosis method based on continuous wavelet transform and deep learning, which strengthened the time-frequency feature modeling effect in blade fault recognition [14]. This kind of research shows that computer vision, time series modeling and deep network have become important technical supports for blade state perception. However, most of the methods still focus on anomaly recognition or fault classification, and the output results are more toward state labels, less directly into the calculation of composite fatigue life and the update of structural parameters.

In terms of the hierarchical damage characterization of composite materials, Khan et al. studied an autonomous evaluation method of laminate delamination based on deep learning and data augmentation, which can automatically identify the hierarchical damage [15]. Zhao et al. proposed a composite damage area localization method based on acoustic emission signal and deep transfer learning, which improved the stability of damage area judgment [16]. Liu et al. studied the composite structure damage detection method by fusing monitoring data and physical mechanism, so that the data-driven model and the structure response mechanism form a collaborative expression [17]. Zhang et al. proposed a damage localization method based on Lamb wave and dense convolutional sparse coding network, which enhanced the mapping ability between fluctuation response and spatial location [18]. Tao et al. proposed a neural fatigue cohesion model integrated with Paris law and applied it to fatigue analysis of open-hole composite laminates, so that the neural network prediction process could embed the

mechanical crack growth law [19]. Perfetto et al. studied the composite plate damage classification method combining guided wave and machine learning, and verified the discrimination effect of different damage categories through experiments [20]. These studies improve the resolution and robustness of damage identification for composite materials, and also provide an important basis for multi-source feature extraction, local degradation representation and health state coding.

As shown in Table 1, most of the existing researches have achieved good results in image recognition, waveform analysis, guided wave classification and local damage detection. However, the research path directly corresponding to fatigue life prediction and optimization of wind turbine blade composite materials still needs to be further closer to the continuous calculation link of "finite element sample - feature mapping - life estimation - parameter optimization".

Table 1: Comparison between existing methods and the technical route of this paper

Reference	Method	Result	Application Boundary
Rizk et al. [11]	Hyperspectral imaging combined with 3D-CNN for blade surface damage detection	Improved recognition accuracy for defects on complex surfaces	Focused on surface detection and did not extend to life estimation
Davis et al. [12]	Deep learning-based blade fault recognition and localization	Achieved unified localization of multiple fault types	Outputs were mainly limited to fault labels
Yang et al. [13]	Joint modeling of blade abnormal states using VAE and Neural ODE	Enhanced continuous representation of state evolution	Lacked an optimization stage for structural parameters
Sethi et al. [14]	Vibration diagnosis combining continuous wavelet transform and deep learning	Strengthened discriminative capability of time-frequency features	Mainly served fault diagnosis tasks
Khan et al. [15]; Zhao et al. [16]	Deep learning and transfer learning for hierarchical recognition and regional localization	Improved characterization of local damage in composite materials	Limited coverage for full-scale life mapping
Liu et al. [17]; Zhang et al. [18]	Physics-informed modeling, Lamb waves, and convolutional sparse coding networks	Enhanced the correlation between damage response and spatial location	Still mainly oriented toward detection and localization tasks
Tao et al. [19]	Neural fatigue cohesive model constrained by Paris law	Established the link between fatigue crack propagation and neural prediction	Mainly applied to specimen-level laminated composites
Perfetto et al. [20]	Composite plate damage classification combining guided waves and machine learning	Verified the effectiveness of distinguishing different damage categories	Insufficient support for blade structural-level optimization
This paper	Joint modeling of multi-scale finite element fatigue simulation, feature-mapped prediction, and parameter optimization	Unified structural response computation, life estimation, and design variable search	Oriented toward fatigue life prediction and optimization of wind turbine blade composites

For wind turbine blade composites, the fatigue life is not determined by a single local crack, but is affected by the layup mode, interface performance, regional stress concentration of the main beam, cyclic load amplitude and structural scale transfer effect. It is difficult to construct a prediction model based on only one type of observation signal to fully express the response coupling relationship between levels. The multi-scale finite element simulation

results are organized into learnable samples, and then the feature mapping model is used to complete the life prediction and parameter optimization, which is more suitable for describing the calculation process from local damage accumulation to overall performance attenuation of blade composite materials.

It can be seen from the table that the existing researches have accumulated mature algorithm experience in damage detection, regional localization and anomaly identification. However, the input of most methods is still dominated by images, vibration or guided wave signals, and the joint modeling between finite element response field, paving parameters and fatigue life variables is insufficient. On the basis of related research, this paper introduces multi-scale finite element fatigue simulation, feature mapping prediction and parameter optimization modules, and puts the structural response calculation, life estimation and design variable search in a unified framework, so as to enhance the expression ability of the model for complex nonlinear fatigue behavior, and provide a computable basis for wind turbine blade composite structure optimization. From the perspective of computer method, this path can effectively link finite element solution, sample learning and optimization search, which not only maintains the physical constraints of structural analysis, but also enhances the generalization stability of fatigue life inference. This kind of modeling method is more suitable for the writing orientation of the combination of algorithm and engineering in technical journals. Therefore, the study of finite element driven life prediction and parameter optimization can not only enhance the calculation depth of blade fatigue assessment, but also help to improve the iterative efficiency of structural design, engineering deployment adaptability and the overall output stability control level.

3 Fatigue life prediction and optimization method of wind turbine blade composite material

3.1 Multi-scale finite element fatigue simulation and life sample construction of wind turbine blade composite material

Fatigue response analysis of wind turbine blade composite material is the basic link of life prediction and structural optimization calculation. Under the combined action of variable amplitude wind load, centrifugal load and gravity cycle, the interface between the main beam, web, leading edge reinforcement layer and interlayer will show obvious scale coupling characteristics. The single-level model can provide the local stress distribution, but it is difficult to simultaneously cover the details of the lay-up, the interface degradation and the bending and torsion response of the whole blade. Therefore, in this paper, the multi-scale finite element simulation method is used to uniformly model the key section of the blade, the laminated plate element and the local damage zone, and the fatigue life sample set is formed based on the calculation results. This process not only serves the subsequent training of the lifetime prediction network, but also provides structural response constraints for the parameter optimization module. The research process is shown in Fig. 1.

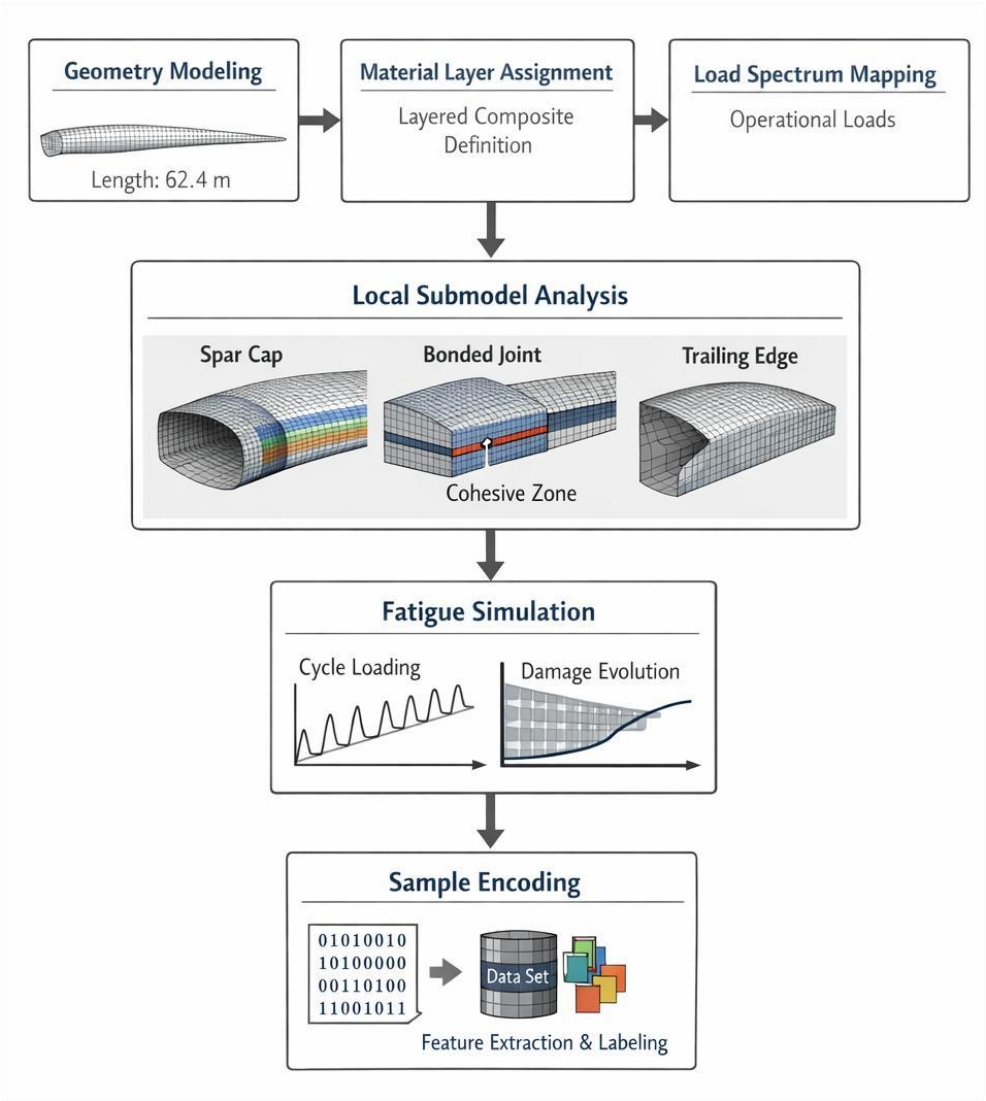

Figure 1: Flowchart of multiscale FEA fatigue simulation and life sample generation

As shown in Fig. 1, the computational flow consists of six parts: geometric modeling, material layered assignment, load spectrum mapping, local submodel unfolding, fatigue cycle solving, and sample coding. The overall blade model was established according to the configuration of 5 MW class onshore wind turbine blades, with a total blade length of 62.4 m, a maximum chord length of 4.31 m, and a root diameter of 3.18 m. The main beam cap, the shear web, the leading edge enhancement layer, and the trailing edge bonding zone were classified as the key analysis regions. The shell element is used to characterize the flexural and torsional coupling response in the global layer, the continuous lamination element is used to describe the directional stress transfer in the local layer, and the cohesion element is used to simulate the initiation and expansion of delemination in the adhesive layer and the interface region. In order to ensure the balance between calculation scale and accuracy, 48216 nodes and 91740 elements are set in the overall blade model, and the local submodels are further refined according to the high strain gradient region. The main modeling parameters are shown in Table 2.

Table 2: Main parameters of the multi-scale finite element model for wind turbine blades

Parameter	Value
Blade Length / m	62.4
Maximum Chord Length / m	4.31
Root Diameter / m	3.18
Number of Shell Elements	68420
Number of Solid Laminated Elements	16780
Number of Cohesive Elements	6540
Longitudinal Elastic Modulus / GPa	41.8
Transverse Elastic Modulus / GPa	12.6
Core Density / ($kg \cdot m^{-3}$)	98
Upper Limit of Design Cycles	1.2×10^{7}

The boundary conditions are set by combining global displacement constraints with local free release. Six degrees of freedom (DOF) constraints were applied to the connection area between the blade root end face and the hub, the blade tip retained bending and torsion free response, and the rotational inertia load was written into the overall model in the form of equivalent physical force. The wind pressure distribution is obtained by interpolating the airfoil profile pressure coefficients along the spanwise direction and mapped to the shell element surface in time steps. For the local submodel, the boundary displacement is not directly set artificially, but is twice transferred by the nodal displacement field of the overall model, so as to maintain the consistency between the interlayer response and the whole blade deformation. This processing method can avoid the stress rise caused by the excessive rigidity of the local model, and also facilitate the unified coding of the displacement trajectories under different working conditions.

In the mesh quality control, a local division strategy is used for the main beam cap Angle, web bonding end and root transition region, and the element aspect ratio is controlled within 2.5 to ensure the numerical stability of the high gradient region. The grid independence check is completed synchronously. The error is controlled within 3%.

The equivalent stiffness of the blade lamination zone is calculated by combining the lamination material orientation matrix with the layup Angle information. In order to compress the response of the multilayer composite at the element level into comparable characteristic variables, the equivalent laminate stiffness expression is used:

$$\bar{A} = \sum_{k=1}^{n} Q^{(k)}(\theta_k)(z_k - z_{k-1}) \tag{1}$$

Here, $\bar{A}$ represents the in-plane equivalent stiffness matrix of the laminates, $Q^{(k)}(\theta_k)$ represents the transformed reduced stiffness matrix of the k layer under the lay-up Angle θ_k, z_k and z_{k-1} represent the thickness coordinates of the upper and lower surfaces of the layer, and n represents the total number of lay-up. Equation (1) is used to transform the layup geometry and material properties into a unified stiffness feature, which is convenient for the subsequent construction of finite element input samples.

The load input is driven by wind speed timing, speed fluctuation and gravity azimuth change. The rated condition, the cut-in to rated transition condition, and the yaw disturbance condition are mapped into three types of cyclic load spectra. In order to describe the cumulative degradation of stress with cycling, this paper introduces a damage evolution variable at the element layer, and updates the fatigue damage using the following equation:

$$D_{t+1} = D_t + \alpha\left(\frac{\Delta\sigma_{eq}}{\sigma_u}\right)^m \left(\frac{N_t}{N_f}\right)^\beta (1 - D_t)^\gamma \quad (2)$$

Here, D_t represents the damage variable at the t cycle step, $\Delta\sigma_{eq}$ represents the equivalent stress amplitude, σ_u represents the ultimate strength of the material, N_t represents the current cumulative number of cycles, N_f represents the number of failure cycles, α, m, β, γ are the material degradation parameters. Equation (2) is used to characterize the continuous effect of stiffness attenuation and interface degradation in the layer on the lifetime response.

In the solution of the local sub-model, the equivalent stress is not directly used as the only criterion, but combined with the strain energy density and the interface cracking displacement to form the risk index. The comprehensive response is written as follows.

$$R_i = \lambda_1 \frac{\sigma_{v,i}}{\sigma_{v,max}} + \lambda_2 \frac{U_i}{U_{max}} + \lambda_3 \frac{\delta_i}{\delta_c} \quad (3)$$

Here, R_i represents the fatigue response index of the i critical element, $\sigma_{v,i}$ represents the Von Mises stress of this element, U_i represents the strain energy density, δ_i represents the interface cracking displacement, δ_c represents the critical cracking displacement, and λ_1 to λ_3 represent the normalized weights. Equation (3) is used to uniformly measure the contribution of different physical quantities to the fatigue damage sensitive area, and is used as the basis for sample screening. The relationship between the critical area grid and the local response is shown in Fig. 2.

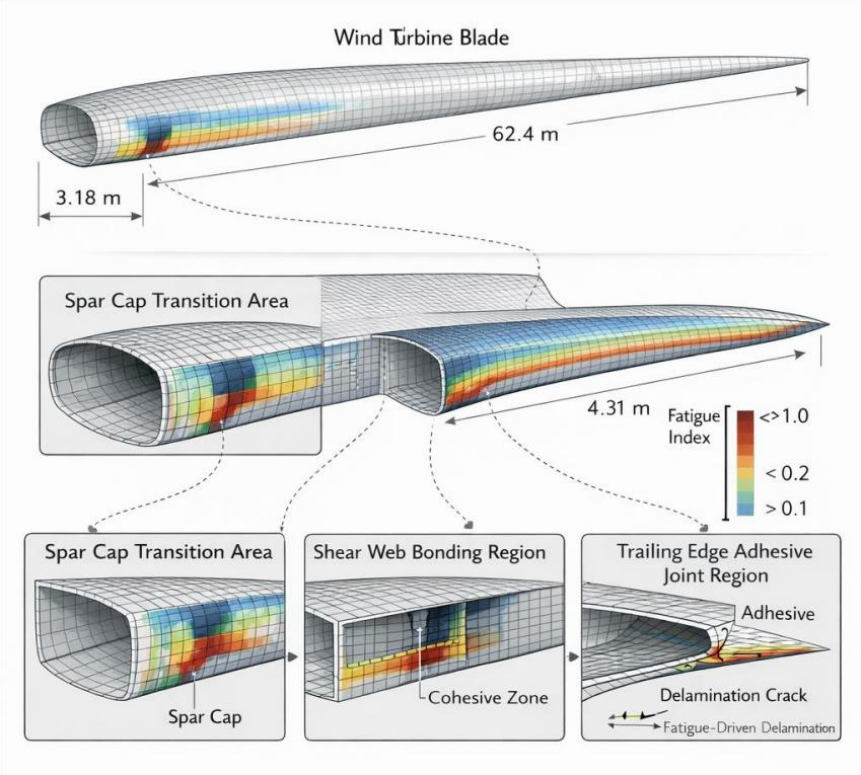

Figure 2: Schematic diagram of the local submodel of the critical section of the blade and the fatigue response region

As shown in Fig. 2, the response index is higher near the turning area of the main beam cap, the web connection area, and near the trailing edge glue wiring. These regions show obvious coupling characteristics of stress concentration and interface displacement under cyclic loading. In order to reduce the proportion of invalid samples, the sensitivity ranking of all candidate parameters is performed after the multi-condition finite element solution is completed in this paper. The initial candidate design variables include girder cap thickness, web thickness, leading edge reinforcement layer thickness, trailing edge adhesive layer thickness, interlayer density, lay-up Angle, and shear web position, with seven items in total. These variables are used for pre-sensitivity analysis and sample amplification to ensure the integrity of parameter space coverage. The central difference form is used to calculate the impact of the response on the design variable:

$$S_j = \frac{F(x_j + \Delta x_j) - F(x_j - \Delta x_j)}{2\Delta x_j}) \tag{4}$$

Here, S_j represents the sensitivity of the j design variable, F represents the lifetime response objective function, x_j represents the value of the design variable, and Δx_j represents the perturbation step size. Equation (4) is used to identify the variables with strong influence on the dual objectives of life and quality, and accordingly reduce the high-dimensional search space.

The sample screening does not stop at the response extremum extraction stage. In order to enhance the adaptability of the subsequent network to the fluctuation of working conditions, this paper further calculated the damage gradient, stiffness reduction rate and dangerous zone migration distance of each group of samples in the early, middle and near failure stages of the cycle, and added them as time series statistical features to the sample vector. In this way, the finite element results are no longer just static result sets, but are transformed into structured data containing both spatial distribution, evolution rate and lifetime labels. Through this process, the model training stage can simultaneously read the material level information, component level response and overall life results, which provides more stable data support for subsequent feature mapping and parameter optimization.

In the sample construction stage, this paper combines Latin hypercube sampling with condition amplification to generate candidate combinations, and encodes the finite element output results into a unified sample vector. A single sample contains six types of information: geometric parameters, material parameters, load spectrum statistics, critical element response index, cumulative damage value and residual life label. A total of 1680 groups of initial samples were obtained, and 1426 groups were retained after eliminating the combinations that did not meet the manufacturing constraints and strength constraints, including 1120 groups of training samples and 306 groups of validation samples. After coding, the samples enter the subsequent feature mapping network, so that the finite element calculation results can be transformed from traditional off-line analysis into a learnable, searchable, and optimized structure life data basis.

3.2 Fatigue life prediction and parameter optimization module design based on finite element feature mapping

After obtaining the multiscale FE samples, it is necessary to establish the mapping module that can complete the lifetime prediction and parameter search. The finite element results include many variables, such as layup Angle, thickness, interface damage, strain energy density, maximum principal stress and cyclic load spectrum, which have high dimension and

strong correlation. If directly used in optimization calculation, the search efficiency will decrease. To this end, this paper constructs a fatigue life prediction and parameter optimization module based on finite element feature mapping, which connects sample coding, feature compression, life regression and constraint optimization into a unified calculation process. Fig. 3 shows the overall structure of the module.

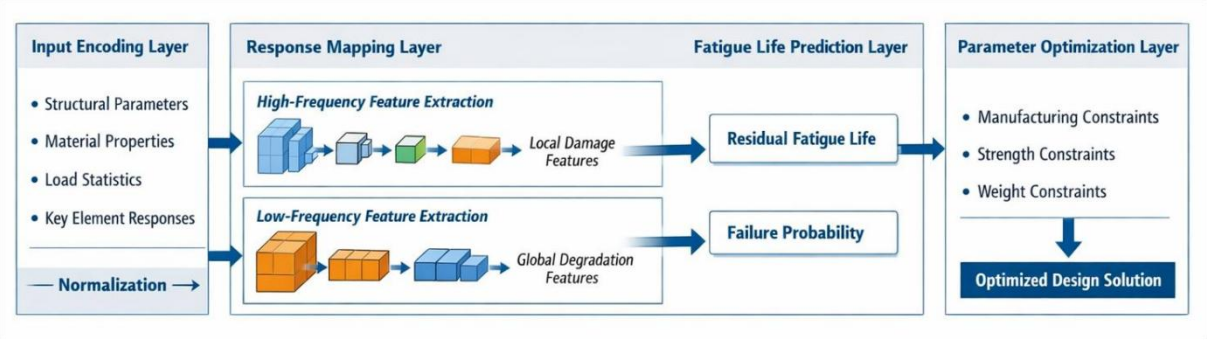

Figure 3: Flowchart of the lifetime prediction and parameter optimization module of the finite element feature map

As shown in Fig. 3, the module consists of an input encoding layer, a response mapping layer, a lifetime prediction layer, and a parameter optimization layer. The input encoding layer receives the structural parameters, material parameters, load statistics, and key element responses from the previous text, which are normalized according to a unified scale. The response mapping layer adopts a double-branch structure, one branch extracts high-frequency features related to local damage, and the other branch extracts low-frequency features related to global stiffness degradation, and then completes the splicing at the fusion node. The life prediction layer outputs the residual fatigue life and failure probability, and the parameter optimization layer searches for a better design combination under manufacturing constraints, strength constraints, and quality constraints. This structure not only preserves the physical meaning of the finite element samples, but also provides a stable numerical foundation for subsequent training.

In order to ensure that different dimensional variables can participate in the training in the same network, this paper adopts the grouping mapping method for the input samples. The geometric parameters, material parameters and load spectrum parameters are represented as static vectors, while the damage evolution and stiffness reduction rate are represented as stage vectors. The encoding expression is as follows:

$$z_i = [W_s x_i^{(s)} + b_s] \,\|\, [W_t \sum_{\tau=1}^{T} \alpha_{i\tau} x_{i\tau}^{(t)} + b_t] \tag{5}$$

Here, z_i represents the unified coding vector of the i sample, $x_i^{(s)}$ represents the static parameter vector, $x_{i\tau}^{(t)}$ represents the timing characteristics of the τ fatigue stage, $\alpha_{i\tau}$ represents the stage weight, W_s, W_t and b_s, b_t represent the mapping weight and bias respectively, $\|$ represents the vector splicing operation. Equation (5) transforms the original finite element sample from the discrete solution result into a network readable feature sequence, which is used to maintain the consistency between the local response and the overall lifetime label.

After completing the initial coding, the module further constructs the response weight matrix to distinguish the contribution of high and low sensitive variables to lifetime prediction.

The weights are not set manually, but are automatically updated by the training phase based on error feedback. The goal is to weaken the disturbance of redundant variables on the convergence path of the network and highlight the key design factors such as the thickness of the main beam cap, the position of the web, the lay-up Angle and the thickness of the rubber layer. The corresponding feature relabeling formula is as follows.

$$\tilde{h}_i = \sigma(W_2\,\phi(W_1 z_i + b_1) + b_2) \odot z_i \tag{6}$$

Here, $\tilde{h}_i$ represents the recalified latent vector, $\sigma(\cdot)$ represents the Sigmoid function, $\phi(\cdot)$ represents the ReLU activation function, W_1, W_2 and b_1, b_2 are gated mapping parameters, $\odot$ represents element-wise multiplication. Equation (6) uses gated mapping to compress invalid dimensions, so that the network can still maintain stable gradient transfer under the condition of mini-batch training.

Fig. 4 shows the internal structure of the feature mapping module. In the figure, the left side shows the static parameter branch, the middle part shows the fatigue stage branch, and the right side shows the fusion output. The two branches merge after the convolutional map and the fully connected map, and generate a unified hidden vector representation. This latent vector is involved in both lifetime regression and objective evaluation in parameter optimization.

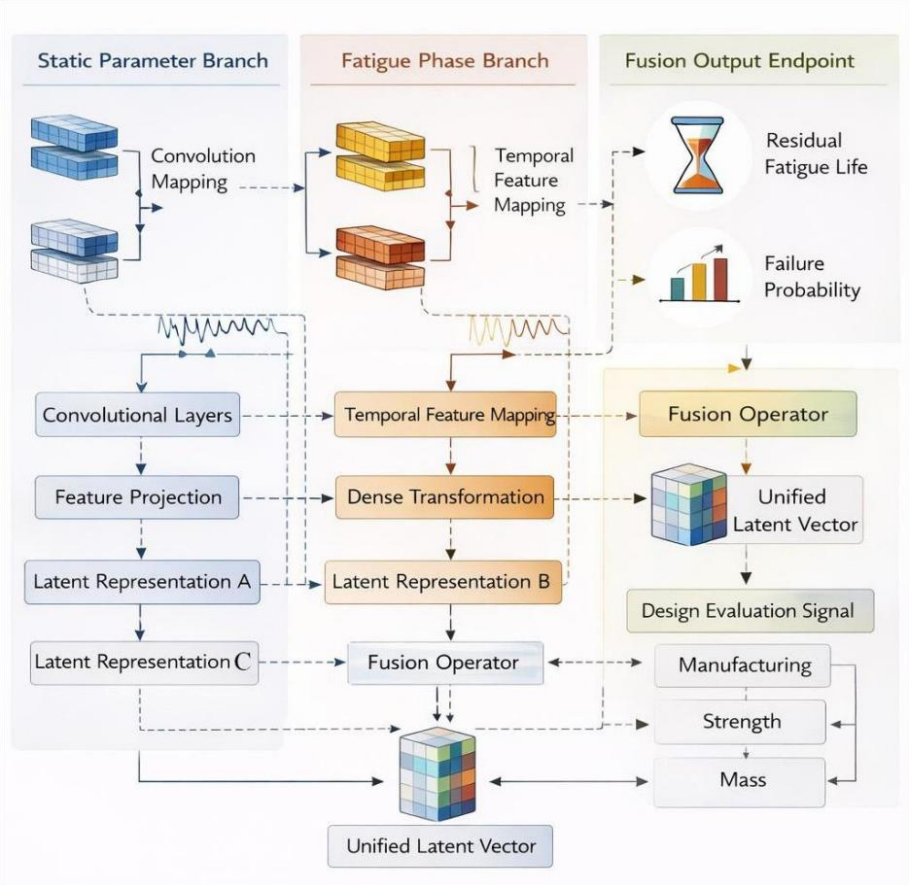

Figure 4: Structure diagram of the two-branch finite element feature mapping network

In the life prediction layer, this paper does not use a single regression head to directly output the cycle life, but constructs a double output structure of life value and failure probability. The reason for this treatment is that the fatigue response of composite material

has obvious nonlinear acceleration characteristics near the failure stage, and it is difficult to completely express the state change only depending on a continuous value. The life prediction formula is as follows:

$$\hat{N}_i = \exp\left(w_N^T \tilde{h}_i + b_N\right), \quad \hat{p}_i = \frac{1}{1 + \exp\left[-\left(w_p^T \tilde{h}_i + b_p\right)\right]} \tag{7}$$

Here, $\hat{N}_i$ represents the predicted residual fatigue life of the i sample, $\hat{p}_i$ represents the corresponding failure probability, w_N and w_p are the output layer weights, b_N andb_p are the bias terms. Equation (7) jointly projects the mapping features, loading statistics and local damage states into the life space, so that the network can maintain the discrimination ability for different load conditions.

In order to enhance the training stability, this paper uses a joint loss function to simultaneously constrain the lifetime error, the probability error and the parameter smoothing term. This processing method can avoid the fitting behavior of the model with excessive deviation on a few extreme samples. The relevant objective function is as follows:

$$\mathcal{L} = \lambda_1 \frac{1}{B} \sum_{i=1}^{B} \left| \ln(\hat{N}_i + 1) - \ln(N_i + 1) \right|$$
$$+ \lambda_2 \frac{1}{B} \sum_{i=1}^{B} \left[-y_i \ln \hat{p}_i - (1 - y_i) \ln(1 - \hat{p}_i) \right] + \lambda_3 \|\Theta\|_2^2 \tag{8}$$

Here, $\mathcal{L}$ represents the total loss, B represents the batch sample number, N_i represents the true lifetime label, y_i represents the failure class label, Θ represents all trainable parameters, and λ_1 to λ_3 represent the loss weights. In Equation (8), logarithmic error is used for the life term, cross entropy is used for the probability term, and two-norm regularization is used for the smoothness term to maintain the continuity of the prediction curve and controllability of parameter update. The training process is shown in Fig. 5.

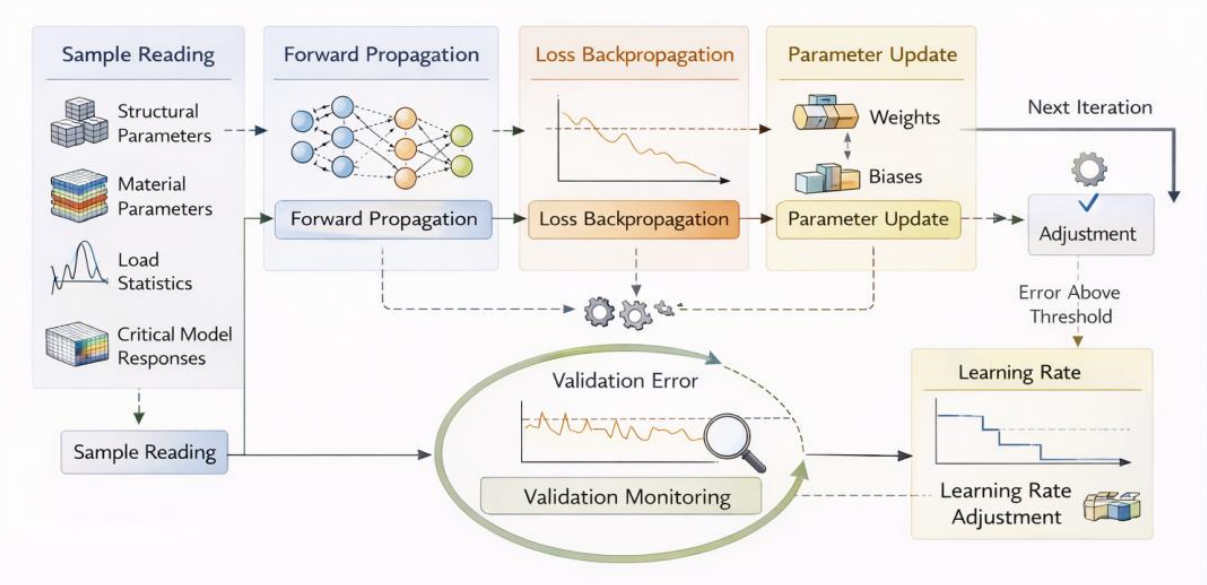

Figure 5: Diagram of co-training process between lifetime prediction network and parameter search

As shown in Fig. 5, the network successively completes sample reading, forward propagation, loss backpropagation, and parameter update in each iteration. The validation set error was continuously monitored before reaching the set threshold, and the learning rate was automatically reduced if there was no significant decrease in successive rounds. Such a setting is beneficial to reduce the oscillation phenomenon when the number of finite element samples is limited, and to ensure the expression ability of the model for different fatigue stages.

In the parameter optimization layer, the minimum blade mass and the maximum fatigue life are taken as the double objectives, and the maximum equivalent stress, interface cracking displacement and manufacturing thickness interval are set as constraints. Due to the coupling relationship between the design variables, the multi-strategy adaptive particle search method is used to complete the optimization. The particle position is composed of thickness, lay-up Angle and web position, and the fitness value is calculated in real time by the lifetime prediction network. The corresponding multi-objective evaluation function is as follows.

$$J(X) = \omega_1 \frac{M(X)}{M_0} - \omega_2 \frac{\widehat{N}(X)}{N_0} + \omega_3 \max\left(0, \frac{\sigma_{eq}(X)}{\sigma_{allow}} - 1\right)^2 + \omega_4 \max\left(0, \frac{\delta(X)}{\delta_{allow}} - 1\right)^2 \quad (9)$$

Where $J(X)$ represents the comprehensive target value of design variable X, $M(X)$ represents the blade mass, $\widehat{N}(X)$ represents the predicted life, M_0 and N_0 are normalized reference values, $\sigma_{eq}(X)$ represents the maximum equivalent stress, σ_{allow} represents the allowable stress,$\delta(X)$ represents the interface cracking displacement, δ_{allow} represents the allowable displacement. ω_1 to ω_4 are the weight coefficients. In Equation (9), the lifetime benefit, quality cost and strength penalty are uniformly written into the objective space, so that the parameter search not only has engineering feasibility, but also maintains good computational efficiency.

In the particle update phase, three mechanisms are introduced: inertial attenuation, local cooperation and boundary rebound. Inertial attenuation is used to control the early search range, local cooperation is used to strengthen the search density near the dominant particle, and boundary rebound is used to avoid the thickness variable from exceeding the manufacturing interval. The particle position update formula is as follows.

$$\begin{aligned} v_i^{k+1} &= \eta_k v_i^k + c_1 r_1 (p_i^k - x_i^k) + c_2 r_2 (g^k - x_i^k) \\ &+ c_3 r_3 (l_i^k - x_i^k), \quad x_i^{k+1} = \Pi_\Omega\left(x_i^k + v_i^{k+1} + \rho_k (x_i^k - x_i^{k-1})\right) \end{aligned} \quad (10)$$

Here, v_i^k and x_i^k represent the velocity and position of the i particle in the k round respectively, η_k represents the inertia coefficient, p_i^k represents the individual optimal position, g^k represents the global optimal position, l_i^k represents the local neighborhood optimal position, c_1 to c_3 represents the learning factor, r_1 to r_3 represents the random number, ρ_k represents the rebound coefficient. Let $\Pi_\Omega(\cdot)$denote the projection operation on the feasible region Ω. The adaptive coefficient in Equation (10) is adjusted with the number of iterations, which can expand the search range in the early stage and improve the convergence accuracy in the later stage.

In addition, the module sets an outlier suppression step before the sample enters the network. If the local element stress, strain energy density, or interface cracking displacement exceeded three standard deviations of the number of bits in the training set, a joint process of piecewise truncation and rescaling was used to avoid extreme samples dominating the parameter update. For the missing stage variables, the interpolation results of adjacent load levels are used to complete, so as to ensure that the input sequence length is consistent. This

preprocessing step improves the compatibility of the finite element samples in the network and also enables the subsequent optimization module to read the prediction results stably. At the same time, the lifetime value output by the module will be compared online with the finite element reference lifetime. If the deviation continuously exceeds the set threshold, the parameter rollback and learning rate reset mechanism will be triggered to maintain the repeatability of the training process and the stability of engineering deployment. This setting ensures that the prediction results are continuously credible.

Table 3 lists the main training and optimization parameters of the module. As can be seen from the table, the lifetime prediction network uses AdamW optimizer, the initial learning rate is set to 0.0005, the batch size is 32, and the maximum number of training rounds is 240. The particle swarm size is set to 40, the maximum number of iterations is 180, and the design variable dimension is 5. The above parameters are determined after repeated testing on the validation set, which can achieve a relatively balanced result between prediction accuracy and computational cost.

Table 3: Fatigue life prediction and parameter optimization module parameter Settings

Module	Parameter	Value
Input Encoding Layer	Static Feature Dimension	18
Input Encoding Layer	Stage Feature Dimension	12
Response Mapping Layer	Hidden Layer Width	64
Response Mapping Layer	Activation Function	ReLU
Life Prediction Layer	Number of Output Heads	2
Training Settings	Optimizer	AdamW
Training Settings	Initial Learning Rate	0.0005
Training Settings	Batch Size	32
Training Settings	Maximum Number of Training Epochs	240
Parameter Optimization Layer	Swarm Size	40
Parameter Optimization Layer	Maximum Number of Iterations	180
Parameter Optimization Layer	Design Variable Dimension	5

With the above design, the finite element solution, feature mapping, lifetime prediction and parameter search are no longer separated from each other, but form a unified computational link. This module can transform the complex composite response results into trainable, regressible and optimizable digital expressions, and provide a consistent data interface for training process analysis, life result verification and structural parameter comparison in Chapter 4. Therefore, the fatigue life prediction and optimization of wind turbine blade composite materials have changed from simple off-line simulation to collaborative solution process oriented to computational model.

4 Experimental Results

4.1 Model training process and convergence characteristics analysis

In this study, Python3.10 and PyTorch2.2 were used to train and analyze the fatigue life prediction module, and the validation set error, objective function change and gradient stability were used as the convergence criteria. The training samples were 1120 groups, and the validation samples were 306 groups. The BP regression network and the mapping network without feature recalibration were selected as the comparison model. AdamW optimizer was

uniformly used in the training phase, the initial learning rate was set to 0.0005, the batch size was 32, the maximum number of training rounds was 240, and the weight decay coefficient was set to 0.0001.

To ensure the consistency of finite element response input under different working conditions, all samples were processed by normalization, outlier truncation and timing completion before entering the network. In order to further illustrate the differences in convergence speed and stability of the constructed models in the training stage, this paper supplementary draws a comparison diagram of the training convergence curves of different models, as shown in Fig. 6. The training results show that the proposed model forms a continuous downward trend after the 28th round, the main loss drops below 0.032 after the 64th round, the error of the validation set is basically stable after the 91st round, and the overall convergence speed is significantly faster than that of the two groups of comparison models. The BP regression network still has large fluctuations near the 120th round. Although the mapping network without aggravating calibration can maintain a decline, the error reduction rate is weakened after the 80th round, which indicates that feature compression and weight allocation have an obvious role in promoting the learning of high-dimensional finite element variables.

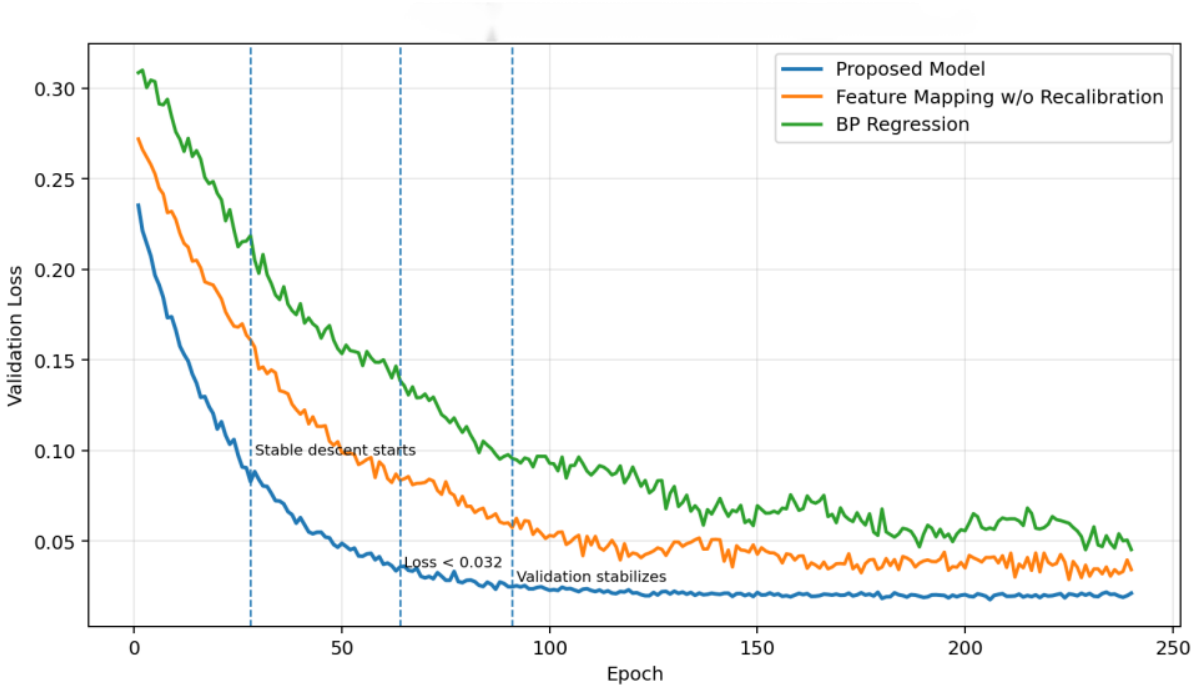

Figure 6: Comparison plots of training convergence curves for different models

Further statistics of the gradient norm change can be found that the gradient mean of the proposed model always maintains between 0.41 and 0.58, and there is no sudden increase or abnormal attenuation, indicating that the dual-branch mapping structure can buffer the scale difference between local damage features and global stiffness features. The comparison model shows short-time oscillations around round 35 and 47, respectively, indicating that the response of the network to highly sensitive variables is still unstable.

With the increase of training rounds, the fitting slope of the proposed model in the medium life interval and the high life interval gradually approached the reference value, and the discretization error band significantly contracted. At the 100th round, the mean absolute percentage error of the training set is reduced to 5.12%, and the error of the validation set is

reduced to 5.44%, which are lower than those of the comparison model. It can be seen that the constructed finite element feature mapping module performs well in terms of convergence speed, training stability and lifetime regression consistency, which can provide a reliable prediction basis for subsequent parameter optimization.

At the same time, the early stopping mechanism and the learning rate backoff strategy weaken the interference of local oscillation on the parameter update in the later stage, so that the network maintains stable output continuity and generalization ability under different fatigue stages. The results show that the model has good numerical robustness and engineering deployment adaptability.

4.2 Verification of fatigue life prediction results of wind turbine blade composite materials

In this study, the fatigue life prediction results were verified on the independent test set, and the test sample consisted of three types of load conditions, namely rated load, variable pitch disturbance load and yaw coupling load, with a total of 306 groups. In order to ensure the comparability of the verification results, this paper compares the proposed finite element feature mapping model with the BP regression network, random forest regression model and LSTM time series regression model, using the same training set, the same normalization method and the same life label definition. The residual fatigue life, relative error and interval hit rate are used as the main evaluation parameters in the prediction output, and the tracking ability of the model to the structural degradation process is judged by combining the stress response of the key region.

Table 4 shows the RMSE, MAPE, R-², and interval hit rate of the four methods on the test set. It can be seen that the RMSE of the proposed model is 0.041, the MAPE is 4.87%, the R^2 reaches 0.941, and the interval hit rate is 93.5%, which are better than the three comparison methods. The MAPE of BP regression network is 8.96%, LSTM model is 6.21%, and random forest model is 7.34%. This shows that after the multi-scale finite element samples enter the unified mapping space, the life regression does not rely on a single statistical correlation, but can use the layup parameters, damage evolution and load spectrum characteristics to complete the joint discrimination.

Table 4: Fatigue life prediction indices of different models on the test set

Method	RMSE	MAPE / %	R^2	Interval Hit Rate / %
Proposed Model	0.041	4.87	0.941	93.5
BP Regression Network	0.083	8.96	0.872	81.4
Random Forest Regression	0.069	7.34	0.894	85.7
LSTM Time-Series Regression	0.055	6.21	0.913	89.6

In order to visually compare the correspondence between the predicted value and the true value, this paper draws the scatter distribution of the test set lifetime prediction, as shown in Fig. 7. It is expressed by using the true life as the horizontal axis and the predicted life as the vertical axis. The results show that the scatter of the proposed model is mainly concentrated near the reference diagonal, and the dispersion degree of the medium lifetime interval and the high lifetime interval is significantly smaller than that of the comparison model. In particular, there is no continuous deviation zone in the model within the cycle interval of 4.0×10^5 to 7.5×10^5, which indicates that the finite element feature mapping can well maintain the correspondence between the local damage index and the overall life. The BP regression network is significantly underestimated in the high lifetime interval, the LSTM model is

locally overestimated in the low lifetime interval, and the random forest model shows a step-like dispersion in the middle interval. This result shows that the proposed model has better fitting consistency under the condition of continuous distribution of lifetime values.

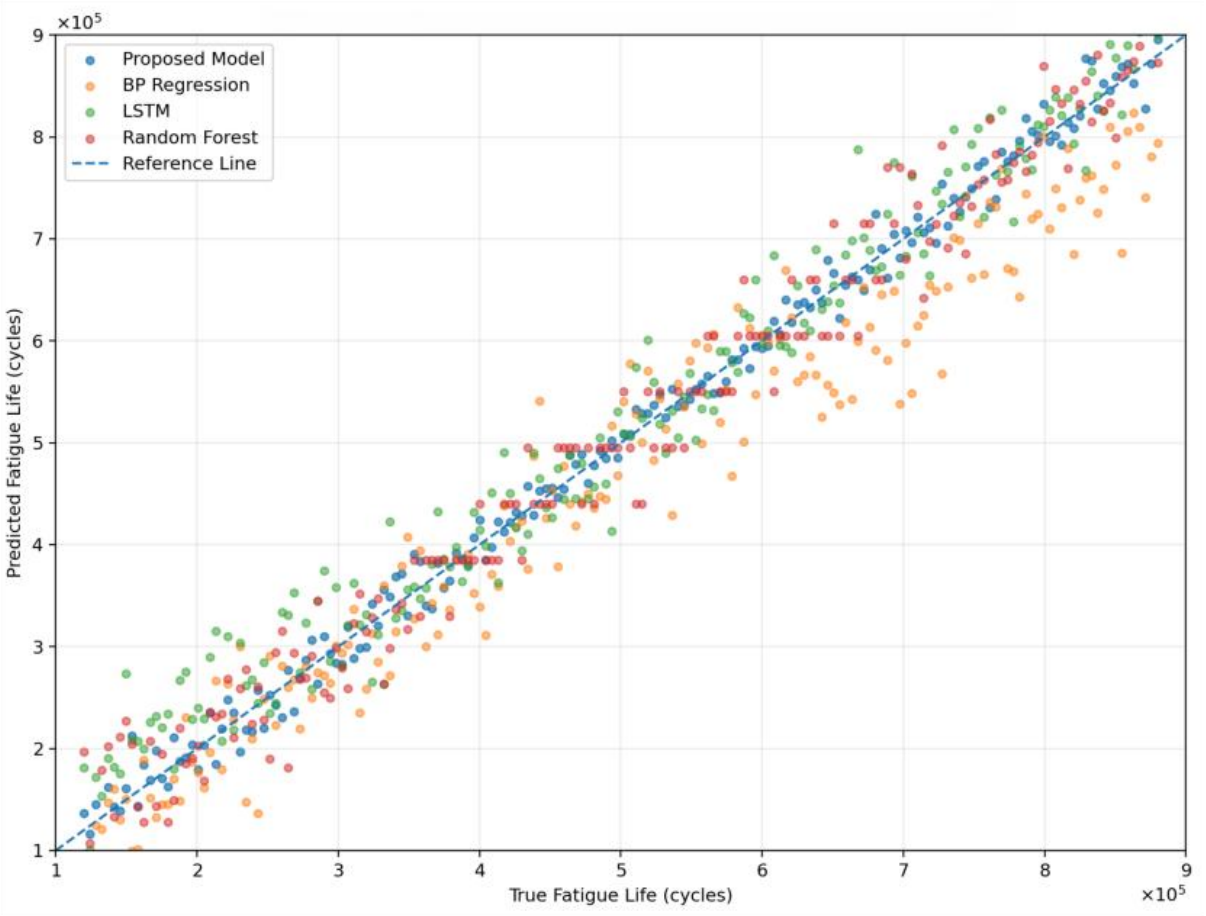

Figure 7: Scatter plot of fatigue life prediction for the test set

In order to further analyze the error stability of the model under different working conditions, box plots of the relative errors under three types of load conditions are further drawn, as shown in Fig. 8. The median errors of the proposed model under rated load, variable pitch disturbance load and yaw coupling load are 4.1%, 4.8% and 5.3%, respectively. The interquartile range is always controlled within 2.6%, and the box length is shorter than that of the other models. This result shows that the proposed model still maintains good output concentration under complex load disturbances. Although the random forest model has a small fluctuation under the rated load, the number of outliers increases under the yaw coupling condition, which reflects the limited adaptability of the tree model to the non-stationary fatigue characteristics. In contrast, the error bands of the proposed model vary gently under the three types of operating conditions, indicating that it has good robustness to the lifetime offset caused by load fluctuations.

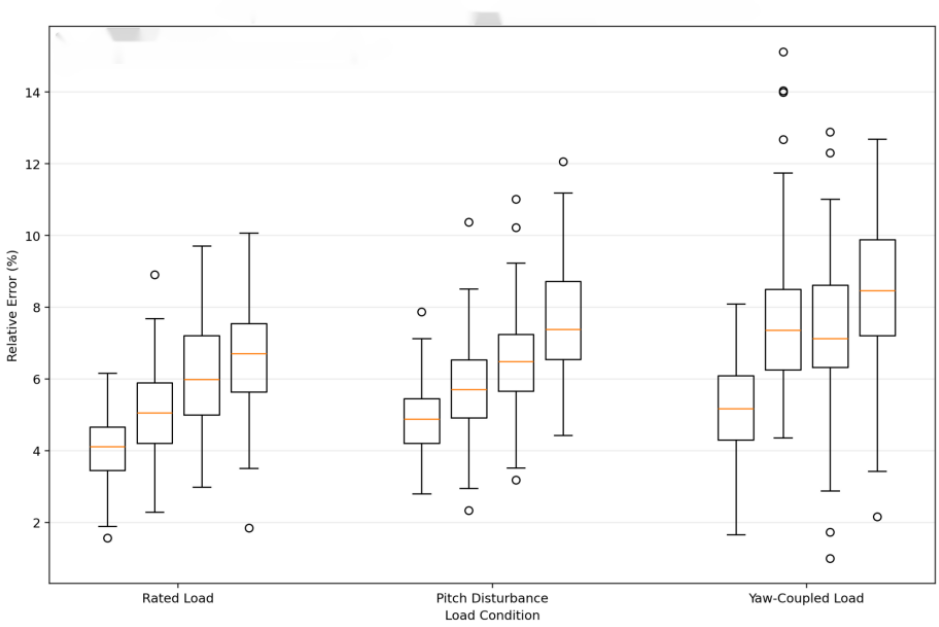

Figure 8: Box plots of relative errors under different loading conditions

In this paper, the interval hits between different fatigue stages and critical regions are also counted, and the results are expressed as heatmaps, as shown in Fig. 9. The hit rate of the main beam cap region is the highest in the middle and late stages, reaching 95.2% and 94.7% respectively. The hit rate of the web connection area in the high load stage is 92.8%. The bonding zone of the trailing edge is slightly lower at 90.6%. This distribution indicates that the finite element feature mapping method is more sensitive to the fatigue damage evolution near the main bearing path and can more accurately capture the life change in the critical region. For the local non-uniform degradation regions such as the trailing edge bonding area, the model still maintains an interval hit rate of more than 90%, which indicates that the input features have a good ability to characterize the local interface response.

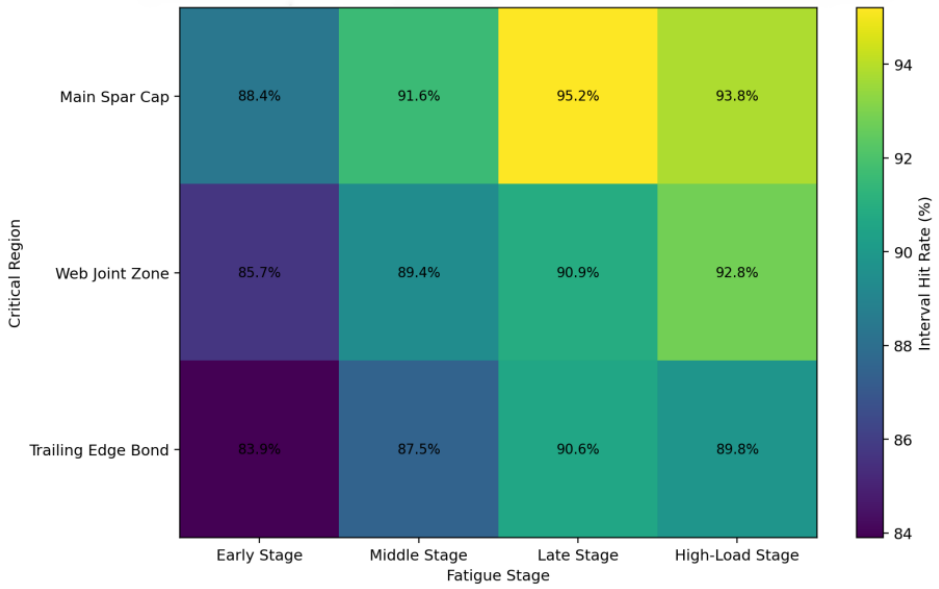

Figure 9: Heat map of fatigue phase versus critical region interval hit rate

Synthesizing the above results, it can be seen that the fatigue life prediction method based on finite element feature mapping has higher regression accuracy, better condition stability and stronger ability to distinguish critical regions on the test set. The proposed method can not only accurately reflect the fatigue life change of wind turbine blade composite materials, but also maintain continuous and stable output characteristics under different load conditions, which provides reliable numerical basis for subsequent blade structural parameter optimization and design variable adjustment.

4.3 Comparison and analysis of wind turbine blade structural parameter optimization results and algorithm

In this section, the finite element feature mapping life prediction module is applied to the structural parameter optimization of wind turbine blades, and the constraint search program is called to complete the solution in the Python environment. According to the sensitivity analysis results above, the core variables entering the optimization module include the thickness of the main beam cap, the position of the web, the thickness of the leading edge enhancement layer, the thickness of the trailing edge adhesive layer and the key lay-up Angle, which are five items in total. The above variables jointly participate in the quality-life bi-objective search and are used as the main update objects in the subsequent finite element review. The optimization objective is set to reduce the blade mass and increase the residual fatigue life while satisfying the strength constraint, displacement constraint and lower limit of life constraint. The change results of key structural parameters before and after optimization are shown in Fig. 10. Fig. 10 mainly shows the changes before and after optimization of four continuous geometric variables. After optimization, the thickness of the main beam cap is reduced from 38.0 mm to 34.5mm, the web spacing is adjusted from 1.62 m to 1.55 m, the thickness of the trailing edge adhesive layer is reduced from 9.0 mm to 7.8 mm, and the thickness of the leading edge enhancement layer is slightly adjusted from 12.5 mm to 13.2 mm. The results show that the proposed method does not simply thin the structure, but establishes a more reasonable parameter allocation relationship between the quality constraint and the lifetime gain.

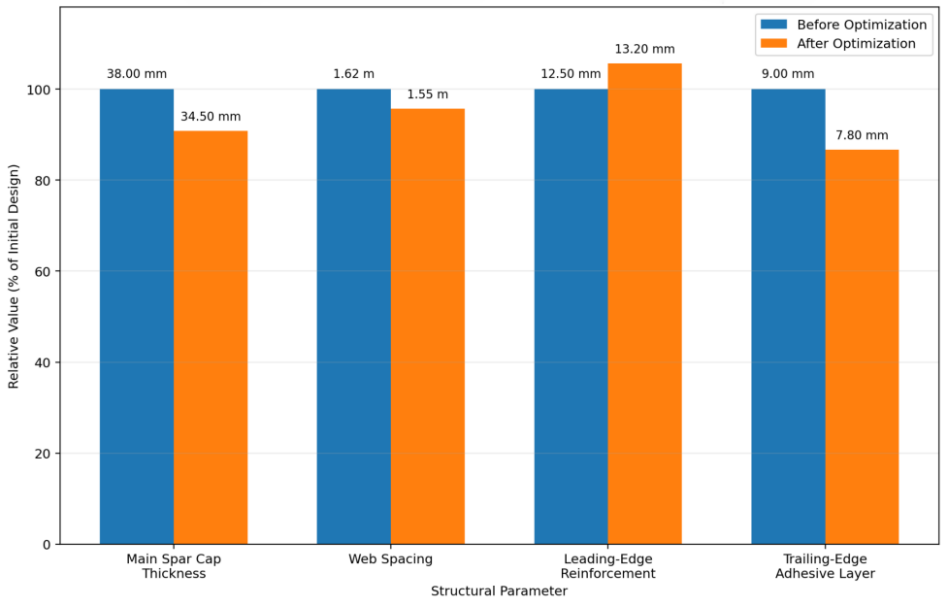

Figure 10: Diagram of key structural parameters change before and after optimization

After the parameter update is completed, this paper further performs a finite element review of the optimization results. The results showed that the total leaf mass decreased from 18.42 t to 17.36 t, with a weight reduction of 5.75%, and the residual life increased from 8.41×10^5 cycles to 9.28×10^5 cycles. The maximum equivalent stress of the main beam cap area increased from 268 MPa to 279 MPa, which was still lower than the allowable value of 305 MPa. The interface cracking displacement of the trailing edge bonding zone is kept within the allowable range of manufacturing and service. The results show that although the optimized structure bears a more concentrated stress response in the local area, the overall bearing capacity is not weakened and the life output is enhanced, which indicates that the finite element feature mapping model can better coordinate the relationship between quality, strength and fatigue life.

In order to compare the output differences of different algorithms in multi-objective search, this paper further plots the quality-lifetime Pareto distribution, as shown in Fig. 11. Compared with PSO, random search and LSTM optimization methods, the solution set obtained by the proposed method is closer to the low-quality, high-lifetime region. When the lifetime target is 9.0×10^5 cycles, the corresponding leaf mass of the proposed method is 17.51 t, which is lower than 17.94 t of the PSO method and 17.73 t of the LSTM method. This indicates that the finite element feature mapping module can not only provide continuous fitness feedback during the search process, but also compress the invalid search area through the lifetime prediction results, thereby improving the efficiency of aggregation of feasible solutions. Compared with random search, the boundary of the solution set obtained by the proposed method is smoother, which indicates that its convergence trajectory in the design variable space is more stable.

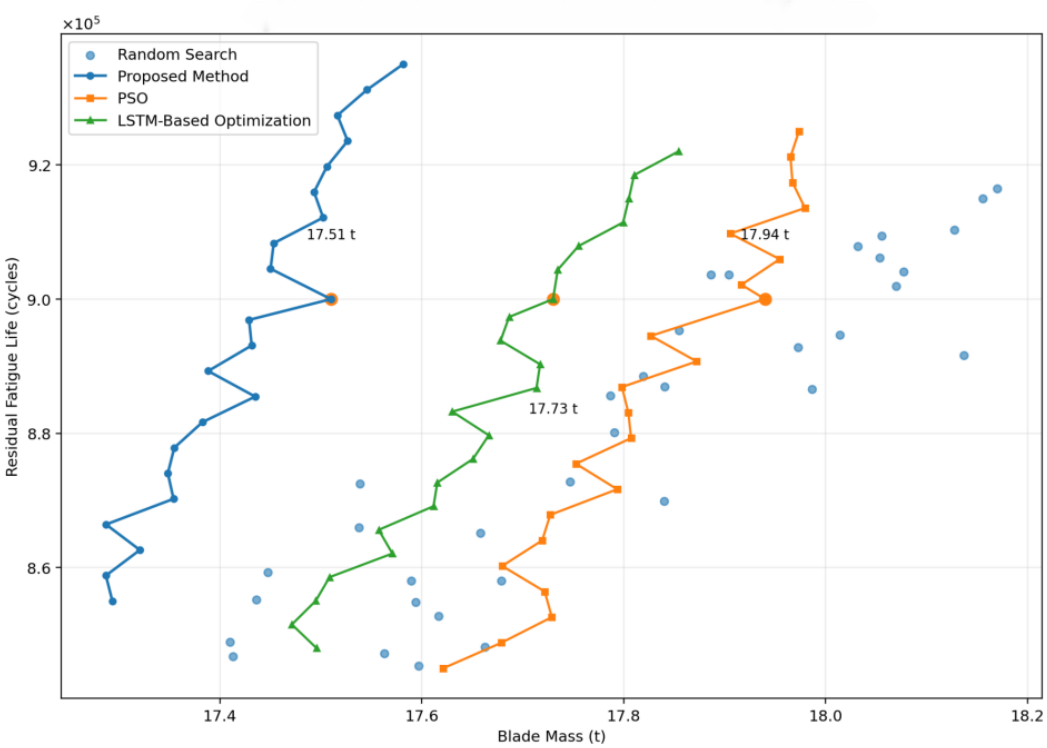

Figure 11: Quality-lifetime Pareto distribution plots for different algorithms

In addition to the overall optimization results, this paper also analyzes the contribution of each component module to the optimization performance through ablation experiments, and the results are shown in Table 5. The lifetime improvement rate, quality reduction rate and

constraint satisfaction rate in Table 5 evaluate the model output from three perspectives of performance gain, lightweighting degree and engineering practicability, respectively. It can be seen that the full model is optimal in all three metrics. After removing the feature re-calibration, the lifetime improvement rate decreases from 10.34% to 7.86%, indicating that the weight adjustment of highly sensitive variables will directly affect the search direction. After removing the dual-output life head, the quality reduction rate can still be maintained at 4.92%, but the constraint satisfaction rate decreases to 91.7%, which indicates that the failure probability branch has a stabilizing effect on the selection of feasible solutions. After removing the adaptive particle update, the distribution of the optimal solution is significantly reduced, and the lifetime improvement rate is further reduced to 6.95%, which indicates that the search strategy has a direct impact on the coverage of the solution space.

Table 5: Results of ablation experiments with different combinations of modules

Model Configuration	Life Improvement Rate / %	Mass Reduction Rate / %	Constraint Satisfaction Rate / %
Full Model	10.34	5.75	96.8
Without Feature Recalibration	7.86	4.88	93.4
Without Dual-Output Life Heads	8.12	4.92	91.7
Without Adaptive Particle Update	6.95	4.37	92.1

Combining the results in Fig.s 10 and 11 and Table 5, it can be seen that the proposed method performs well in terms of structural weight reduction, lifetime gain and constraint consistency, which not only retains the physical constraints of FE analysis, but also enhances the computational efficiency of parameter search. The results show that the optimization framework based on finite element feature mapping can provide more stable computational support for wind turbine blade composite structure design, and has good adaptability for engineering deployment.

5 Discussion

The results of this paper show that the fatigue life prediction and parameter optimization framework based on finite element feature mapping has good computational stability and engineering adaptability in the wind turbine blade composite material scenario. In the training stage, the verification error of the model tends to be stable after the 91through, and the mean gradient is maintained between 0.41 and 0.58, indicating that the dual-branch mapping structure can effectively coordinate the local damage characteristics and the global stiffness degradation characteristics. In the test stage, the MAPE of the model is 4.87%, the R^2 is 0.941, and the interval hit rate is 93.5%. It shows that the finite element samples can accurately maintain the nonlinear correspondence between the layup parameters, the interface degradation and the life label after unified coding. The structural optimization results further show that the method does not rely on a single weight reduction strategy to obtain life gain, but forms a more reasonable combination among the girder cap thickness, web position, rubber layer thickness and lay-up Angle. After optimization, the total mass of the blade is reduced by 5.75%, the residual life is increased by 10.34%, and the constraint satisfaction rate is maintained at 96.8%, which indicates that the calculation model can establish a stable balance between the strength boundary, the displacement limit and the life goal. Compared with PSO, random search and LSTM optimization methods, the solution set obtained by the

proposed method is more concentrated in the low-quality and high-lifetime region, which indicates that the feature mapping module has an obvious constraint effect on the search direction. It can be seen that the proposed method establishes a relatively stable mapping relationship between the multi-scale finite element results and the intelligent optimization calculation. The results show that the model can not only maintain the continuity and interpretability of the output, but also has a certain potential for engineering deployment.

6 Conclusions

Focusing on the task of fatigue life prediction and optimization of wind turbine blade composites under multi-scale finite element simulation, a unified computational framework consisting of life sample generation, feature mapping prediction and parameter search is constructed. The results show that the proposed method achieves the simultaneous improvement of life prediction accuracy and optimization efficiency while maintaining the effectiveness of structural constraints. The MAPE of the test set is 4.87% and R^2 is 0.941. The optimized leaf mass is reduced by 5.75% and the residual life is increased by 10.34%. These results show that the finite element response field, damage evolution and design variables can provide a more stable digital expression for wind turbine blade composite life analysis after unified coding. There are still two limitations in this paper. On the one hand, the training samples are mainly from the simulation generated data. Although some validation samples are introduced, the coverage of cross-model, cross-scale and cross-environmental operating conditions is still limited. On the other hand, the current optimization variables focus on thickness, layup Angle and web position, and the online fusion of manufacturing deviation, material dispersion and service monitoring data is not fully considered. Further research can be carried out in three directions: expanding the joint training of measured fatigue samples and digital twin data to enhance the transfer ability of the model; A lightweight graph structure update mechanism was introduced to improve the efficiency of online prediction. Manufacturing constraints, sensing feedback, and adaptive control strategies are incorporated into the same optimization closed loop to improve engineering deployment applicability. At the same time, the follow-up research can further improve the feature interpretation module, enhance the correspondence between the life prediction results and the local damage evolution path, so as to improve the verifiability and engineering support ability of the model.

References

[1] Wang M H, Lu S D, Hsieh C C, et al. Fault detection of wind turbine blades using multi-channel CNN[J]. Sustainability, 2022, 14(3): 1781.

[2] Zhang C, Yang T, Yang J. Image recognition of wind turbine blade defects using attention-based MobileNetv1-YOLOv4 and transfer learning[J]. Sensors, 2022, 22(16): 6009.

[3] Xiaoxun Z, Xinyu H, Xiaoxia G, et al. Research on crack detection method of wind turbine blade based on a deep learning method[J]. Applied Energy, 2022, 328: 120241.

[4] Khazaee M, Derian P, Mouraud A. A comprehensive study on Structural Health Monitoring (SHM) of wind turbine blades by instrumenting tower using machine learning methods[J]. Renewable Energy, 2022, 199: 1568-1579.

[5] Luo K, Chen L, Liang W. Structural health monitoring of carbon fiber reinforced polymer composite laminates for offshore wind turbine blades based on dual maximum correlation coefficient method[J]. Renewable Energy, 2022, 201: 1163-1175.

[6] Ogaili A A F, Jaber A A, Hamzah M N. A methodological approach for detecting multiple faults in wind turbine blades based on vibration signals and machine learning[J]. Curved and Layered Structures, 2023, 10(1): 20220214.

[7] Oliveira-Filho A, Zemouri R, Cambron P, et al. Early detection and diagnosis of wind turbine abnormal conditions using an interpretable supervised variational autoencoder model[J]. Energies, 2023, 16(12): 4544.

[8] Feng W, Yang D, Du W, et al. In situ structural health monitoring of full-scale wind turbine blades in operation based on stereo digital image correlation[J]. Sustainability, 2023, 15(18): 13783.

[9] Hang X, Zhu X, Gao X, et al. Study on crack monitoring method of wind turbine blade based on AI model: Integration of classification, detection, segmentation and fault level evaluation[J]. Renewable Energy, 2024, 224: 120152.

[10] Ye X, Wang L, Huang C, et al. Wind turbine blade defect detection with a semi-supervised deep learning framework[J]. Engineering Applications of Artificial Intelligence, 2024, 136: 108908.

[11] Rizk P, Rizk F, Karganroudi S S, et al. Advanced wind turbine blade inspection with hyperspectral imaging and 3D convolutional neural networks for damage detection[J]. Energy and AI, 2024, 16: 100366.

[12] Davis M, Nazario Dejesus E, Shekaramiz M, et al. Identification and localization of wind turbine blade faults using deep learning[J]. Applied Sciences, 2024, 14(14): 6319.

[13] Yang Z, Xu M, Wang S, et al. Detection of wind turbine blade abnormalities through a deep learning model integrating VAE and neural ODE[J]. Ocean Engineering, 2024, 302: 117689.

[14] Sethi M R, Subba A B, Faisal M, et al. Fault diagnosis of wind turbine blades with continuous wavelet transform based deep learning model using vibration signal[J]. Engineering Applications of Artificial Intelligence, 2024, 138: 109372.

[15] Khan A, Raouf I, Noh Y R, et al. Autonomous assessment of delamination in laminated composites using deep learning and data augmentation[J]. Composite Structures, 2022, 290: 115502.

[16] Zhao J, Xie W, Yu D, et al. Deep transfer learning approach for localization of damage area in composite laminates using acoustic emission signal[J]. Polymers, 2023, 15(6): 1520.

[17] Liu C, Xu X, Wu J, et al. Deep transfer learning-based damage detection of composite structures by fusing monitoring data with physical mechanism[J]. Engineering Applications of Artificial Intelligence, 2023, 123: 106245.

[18] Zhang H, Hua J, Lin J, et al. Damage localization with Lamb waves using dense convolutional sparse coding network[J]. Structural Health Monitoring, 2023, 22(2): 1180-1192.

[19] Tao C, Zhang C, Ji H, et al. A Paris-law-informed neural fatigue cohesive model and its application to open-hole composite laminates[J]. International Journal of Solids and Structures, 2023, 267: 112158.

[20] Perfetto D, Rezazadeh N, Aversano A, et al. Composite panel damage classification based on guided waves and machine learning: an experimental approach[J]. Applied Sciences, 2023, 13(18): 10017.